LANGMUIR
Cite This: *Langmuir* 2018, 34, 4614−4625
Article
pubs.acs.org/Langmuir

Structure−Property Relationships of Amine-rich and Membrane-Disruptive Poly(oxonorbornene)-Coated Gold Nanoparticles

Zheng Zheng,[†] Julia Saar,[‡] Bo Zhi,[§] Tian A. Qiu,[§] Miranda J. Gallagher,[∥] D. Howard Fairbrother,[∥] Christy L. Haynes,[§] Karen Lienkamp,[‡] and Zeev Rosenzweig*[,†]

[†]Department of Chemistry and Biochemistry, University of Maryland Baltimore County, Baltimore, Maryland 21250, United States
[‡]Department of Microsystems Engineering (IMTEK) and Freiburg Center for Interactive Materials and Bioinspired Technologies (FIT), Albert-Ludwigs-Universitat, Freiburg 79085, Germany
[§]Department of Chemistry, University of Minnesota, Minneapolis, Minnesota 55455, United States
[∥]Department of Chemistry, Johns Hopkins University, Baltimore, Maryland 21218, United States

Supporting Information

ABSTRACT: The article describes the interactions between poly (oxonorbornenes) (PONs)-coated gold nanoparticles (AuNPs) with phospholipid vesicles and shows that the strength of these interactions strongly depends on the molecular structure of PONs, specifically their amine/alkyl side chain ratio. PONs, which are a recently introduced class of cationic polyelectrolytes, can be systematically varied to control the amine/alkyl ratio and to explore how the chemical character of cationic polyelectrolytes affects their interactions and the interactions of their nanoparticle conjugates with model membranes. Our study shows that increasing the amine/alkyl ratio by copolymerization of diamine and 1:1 amine/butyl oxonorbornene monomers impacts the availability of PONs amine/ammonium functional groups to interact with phospholipid membranes, the PONs surface coverage on AuNPs, and the membrane disruption activity of free PONs and PONs−AuNPs. The study makes use of transmission electron microscopy, UV−vis spectroscopy, dynamic light scattering, thermogravimetric analysis, fluorescamine assay, ζ-potential measurements, and X-ray photoelectron spectroscopy measurements to characterize the PONs−AuNPs' size, size distribution, aggregation state, surface charge, and PONs surface coverage. The study also makes use of real-time fluorescence measurements of fluorescent liposomes before and during exposure to free PONs and PONs−AuNPs to determine the membrane disruption activity of free PONs and PONs−AuNPs. As commonly observed with cationic polyelectrolytes, both free PONs and PONs−AuNPs display significant membrane disruption activity. Under conditions where the amine/alkyl ratio in PONs maximizes PONs surface coverage, the membrane disruption activity of PONs−AuNPs is about 10-fold higher than the membrane disruption activity of the same free PONs. This is attributed to the increased local concentration of ammonium ions when PONs−AuNPs interact with the liposome membranes. In contrast, the hydrophobicity of amine-rich PONs, which are made for example from diamine oxonorbornene monomers, is significantly reduced. This leads to a significant reduction of PON surface coverage on AuNPs and in turn to a significant decrease in membrane disruption.

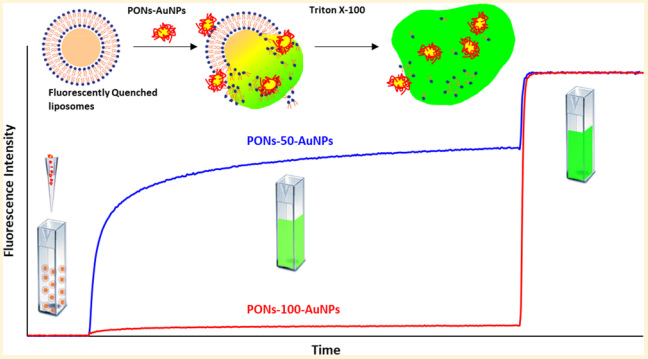

INTRODUCTION

Cationic polymers such as poly(allylamine hydrochloride) (PAH) are often used to coat nanoparticles because they increase the chemical stability of nanoparticles in solution.[1−5] Besides providing aqueous solution stability to nanoparticles, many cationic polymers are also intrinsically membrane-active, particularly against negatively charged membranes. When coating nanoparticles, cationic polymers serve as the interface between the nanoparticles and membranes of cells and organisms. It is therefore crucial to understand the interactions between cationic polymer-coated nanoparticles and phospholipid membranes at the molecular level. This study aims at understanding how variations in the molecular structure of cationic polymers affect the coverage/thickness and morphology of the polymeric coating and the impact of the cationic polymers and their nanoparticle conjugates on phospholipid membranes.

Seminal work by Tirrell and co-workers showed that cationic polymers bind to the anionic components of erythrocytes[6] and to negatively charged liposomes that model the membrane of bacteria.[7−10] These polymers also modulate the interaction of negatively charged lipids with other positively charged

Received: December 19, 2017
Revised: February 22, 2018
Published: March 21, 2018

DOI: 10.1021/acs.langmuir.7b04285
Langmuir 2018, 34, 4614−4625

compounds in biological media, including bivalent counterions like Mg^{2+}.[11,12] This membrane activity, which originates in the positive charge of the polymers, combined with a certain degree of hydrophobicity, renders some cationic polymers antimicrobial. Antimicrobial polymers interact with the anionic parts of membranes, but their disruptive effect on bacterial membranes is driven by their hydrophobicity. For example, the antimicrobial polymer poly(hexamethylene biguanide hydrochloride) (PHMB) binds to negatively charged membranes and causes changes in the membrane composition of liposomes and bacterial cells, which result in bacterial cell death.[13,14] The mechanism of interaction between PHMB and *Escherichia coli* cells is believed to start with PHMB binding to the phosphate head groups of *E. coli*'s outer membrane, which compromises the integrity of that membrane.[15] This allows PHMB to reach and bind to the plasma membrane of *E. coli* cells. The plasma membrane then suffers an increased permeability, which causes an efflux of K^+ ions and stalls bacterial growth. Subsequently, the plasma membrane ruptures, cytoplasmic components precipitate, and the cells die. There is compelling evidence showing that polymers carrying ammonium or phosphonium groups instead of guanidinium groups operate by following a similar mechanism of action. These lines of evidence suggest that cationic polymers interact with the negatively charged membranes of bacterial cells by a nonspecific, nonreceptor-mediated biophysical process, which includes altering membrane fluidity and permeability and the release of membrane-stabilizing ions.

Recent studies have shown that nanoparticles coated with cationic polymers and ligands exhibit similar and sometimes enhanced membrane activity compared to that of free cationic polymers and ligands.[5,16] For example, Rotello and co-workers found that gold nanoparticles (AuNPs) functionalized with cationic ammonium groups disrupt the membranes of Cos-1 kidney cells, red blood cells, and *E. coli* cells nearly an order of magnitude faster than by AuNPs that are functionalized functionalized with anionic carboxylic groups.[16] They found that the increase in membrane lysis does not depend strongly on cell type. This suggests that the interactions between cationic nanoparticles and cell membranes are nonspecific, largely dependent on nanoparticle charge, and do not involve an active uptake process. Klaper and co-workers compared the impact of AuNPs, which were wrapped with the primary amine and quaternary ammonium-rich poly(allylamine hydrochloride) (PAH) and cetyl trimethylammonium bromide (CTAB), and therefore were positively charged at pH 7.0, with with AuNPs, which were functionalized with mercapto-propionic acid (MPA) and citric acid, and therefore were negatively charged at pH 7.0 on the aquatic water flea *Daphnia magna*.[5] The positively charged PAH and CTAB-functionalized AuNPs showed a significantly higher impact on *D. magna* viability than that of the negatively charged MPA and citrate-functionalized AuNPs.[5] While there are many studies showing that the membrane-disruptive effect of cationic polymers increases when the polymers are concentrated on the surface of nanoparticles, systematic studies to assess the impact of the molecular structure of the polymers on the membrane activity of their nanoparticle conjugates have not been carried out, mostly due to the lack of commercially available cationic polymers with systematic structural variations.

The synthesis, antimicrobial activity, and membrane activity of poly(oxonorbornenes) (PONs) were previously reported by Lienkamp and Tew.[17−23] PONs are facially amphiphilic polymers, containing one charged ammonium-terminated side chain and one hydrophobic alkyl side chain on each repeat unit. The primary ammonium group on these polymers is typically in equilibrium with the corresponding amine under physiological conditions. Because they are built from a modular synthesis platform,[17] PONs are amenable to systematic variation of their ammonium/amine density and hydrophobicity, e.g., by varying the length of the alkyl side chain or by synthesizing copolymers with different ratios of diammonium-substituted repeat units and amphiphilic ammonium/alkyl repeat units.[16−18,24,25] PONs with appropriate amphiphilicity were shown to be highly active against bacteria, both as free PONs in solution[17−19,24,25] and as surface-attached PONs networks.[20]

In this work, we investigated the impact of PONs-coated gold nanoparticles (PONs−AuNPs) on negatively charged phospholipid vesicles (liposomes). The first objective of our study was to characterize PONs−AuNPs structurally and chemically with specific emphasis on polymer surface coverage on the nanoparticles. This is imperative to understand the structure−activity relationships of PONs−AuNPs because PONs−AuNPs are a unique and new nanoscale system, which bridges a scale gap in membrane-disruptive activity of free PONs and PONs-coated surfaces. The second objective of our study was to determine whether the increased membrane disruption activity of PAH-coated AuNPs compared to that of PAH, previously reported by Klaper and co-workers,[5] is generalizable to other cationic amine-rich cationic polyelectrolytes. The third objective of our study was to determine whether the relationships between the molecular structure and membrane activity of PONs, which were previously reported by Lienkamp and co-workers for free PONs in solution[17,19,24,25] and on flat surfaces,[20] are maintained when PONs are immobilized on nanoparticle surfaces. Because cationic polyelectrolytes are likely to be used for nanoparticle stabilization in aqueous media and in a broad range of applications including, but not limited to drug delivery, bioimaging agents, and possibly antibacterial agents, it is critically important to understand the fundamental interactions between cationic polymers and nanoparticles and between cationic polymer-coated nanoparticles and model membranes at the molecular level. Molecular-level understanding of these interactions is imperative to the development of environmentally benign synthetic nanoparticles with minimal adverse impact on living organisms.

EXPERIMENTAL METHODS

Reagents for Oxonorbornene Monomer Synthesis and Polymerization. Reagent-grade maleic acid anhydride, furan, 1-butanol, 4-(dimethylamino)pyridine, dicyclohexyl carbodiimide, and *N*-Boc-ethanolamine, which were used for oxonorbornene monomer synthesis, were purchased from Sigma-Aldrich and used as received. Solvents needed for the synthesis including toluene (dry), tetrahydrofurane (dry), dichloromethane (freshly distilled from CaH_2), and *n*-hexane were purchased from Carl Roth. A Grubbs second-generation catalyst was purchased from Sigma-Aldrich; it was reacted with pyridine to form a Grubbs third-generation catalyst using a previously reported procedure.[26] ^{1}H NMR spectra were recorded on a Bruker 250 MHz spectrometer (Bruker, Madison, WI) to confirm the molecular structure of the oxonorbornene monomers and polymers. The molecular mass and mass distribution of the polymers were studied by gel permeation chromatography (GPC) using an Agilent GPC system with chloroform as eluent, PSS SDV columns (PSS, Mainz, Germany), and poly(methyl methacrylate) standards.

Materials and Reagents for AuNPs Synthesis. Gold chloride hydrate and CF300-Cu-50 transmission electron microscopy (TEM)

DOI: 10.1021/acs.langmuir.7b04285
Langmuir 2018, 34, 4614−4625

grids were purchased from Electron Microscopy Services. 4-(2-Hydroxyethyl)piperazine-1-ethanesulfonic acid (HEPES), *O*-(2-carboxyethyl)-*O*′-(2-mercaptoethyl)heptaethylene glycol (HEG), sodium citrate, calcein, sodium phosphate, Triton X-100, CL-4B sepharose, 1-ethyl-3-(3-dimethylaminopropyl) carbodiimide (EDC), and *N*-hydroxy sulfo-succinimide sodium salt (NHS) were purchased from Sigma-Aldrich. Polystyrene disposable cuvettes were purchased from VWR. Millipore deionized water was used in all experiments without further treatment. All reagents and solvents were used as is without further purification.

Materials and Reagents for Liposome Preparation. Palmitoyl-oleoyl phosphatidyl choline (POPC), palmitoyl-oleoyl phosphatidyl glycerol (POPG), and 50 nm pore-size polycarbonate filters were purchased from Avanti Polar Lipids. Surfactant-free cellulose acetate (SFCA) syringe filters were purchased from Corning.

Oxonorbornene Monomer and Polymer Synthesis. The synthesis and purification of oxonorbornene monomers and poly(oxonorbornenes) (PONs) were performed as previously described.[17,19,24,25] A detailed description of the monomer and polymer synthesis is provided in the Supporting Information. In this study, we synthesized and used PONs with varying amine/alkyl side chain ratios between 50 and 100%.

AuNPs Synthesis. AuNPs with an average diameter of 32 nm were synthesized by reducing gold chloride hydrate with sodium citrate following procedures by Jana et al.[27] Briefly, 5 mL of 40 mM $HAuCl_4 \cdot H_2O$ was added to 800 mL of deionized water and the solution was heated to 100 °C. Next, 16 mL of 5% (w/w) (0.17 M) sodium citrate was added and the reaction temperature was lowered to 90 °C. The solution was stirred for 30 min. An additional 4 mL of 5% (w/w) sodium citrate was added, and the solution was stirred for 10 min. AuNP formation was indicated by the appearance of a deep red color. The AuNP solution was allowed to cool to room temperature before use. For purification, the AuNPs were centrifuged at 20 000 RCF (RCF = relative centrifugal force in *g*'s) for 15 min while keeping the temperature constant at 25 °C. They were then resuspended in Milli-Q water and filtered through a 0.45 μm SFCA syringe filter. A UV−vis spectrum was recorded to determine the AuNP concentration, and the solution was diluted to 5 nM AuNPs for further use.

Conjugation of PONs to AuNPs Using EDC Coupling. A 22 mM HEG solution (200 μL) in Milli-Q water was added to 10 mL of a 5 nM solution of AuNPs, and the solution was vortexed for 1 min. The reaction mixture was incubated overnight at room temperature. The resulting HEG−AuNPs were washed by a 15 min long centrifugation at 6500 RCF and 25 °C, which was followed by resuspension in 10 mL of Milli-Q water that was adjusted to a pH of 11 using 1 M NaOH. The centrifugation speed was minimized to enable AuNP precipitation while maintaining the structural integrity of HEG and later PONs on the AuNP surface. The solution was filtered through a 0.45 μm SFCA syringe filter (Corning), and the AuNPs' concentration was adjusted to 5 nM using pH 11 Millipore water. PONs-coated AuNPs (PONs−AuNPs) were synthesized by adding 800 μL of 5 nM HEG-functionalized AuNPs to 19.2 mL of 0.01 M HEPES buffer at pH 6.0. The solution was stirred rapidly, and 50 μL of 0.2 M EDC and 100 μL of 0.2 M sulfo-NHS were added simultaneously to the AuNPs solution. Then, 100 μL of 3.3 mM PONs in DMSO was added to initiate the conjugation of PONs to AuNPs through the formation of amide bonds between the amine-rich PONs and the AuNPs carboxyl groups. The solution was stirred for 6 h at room temperature. The PONs−AuNPs were then washed to remove excess reactants by three cycles of centrifugation at 1650 RFC for 20 min at 25 °C and resuspension in 10 mL of 10 mM HEPES buffer at pH 6.0. PONs−AuNP solutions were stored under mildly acidic conditions (slightly outside the HEPES buffer useful range) to maximize stability. All assays were conducted at pH 7.0 within the useful range of the HEPES buffer.

Liposome Preparation. Liposomes were prepared using a dehydration/rehydration method, which is often employed to form unilamellar liposomes with an overall diameter of 50−100 nm.[28] Liposome preparation involved mixing POPC/POPG (1 mL of 25 mg mL^{-1} POPC/0.25 mL of 10 mg mL^{-1} POPG in chloroform inside a 200 mL round bottom flask, resulting in a 10:1 molar ratio). The phospholipid solution was dried with a stream of N_2 to form a film on the bottom of the flask and further dried under high vacuum overnight. The dried phospholipids were resuspended in a 2 mL solution of 25 mM calcein sodium salt in 10 mM HEPES buffer at pH 7. The phospholipid solution was freeze−thawed between a −80 °C dry ice acetone bath and a 25 °C water bath. The liposomes were then extruded using a polycarbonate membrane with a pore size of 50 nm to induce the formation of unilamellar liposomes with a precise diameter. Size exclusion column chromatography was used to separate dye-containing liposomes from the free dye. Free fluorophore molecules were removed by loading 200 μL of the extruded solution onto a Sepharose CL-4B column (10 mm × 100 mm). The samples were eluted with 1.5 mL of 10 mM HEPES buffer at pH 7.0. Liposomes appear as a faint brown/orange band that elutes before the free fluorophores.

Transmission Electron Microscopy. Samples of PONs−AuNPs (10 μL) were pipetted onto a TEM grid (CF300-Cu-50, EMS) and allowed to air dry. Then, the samples were imaged using a 100 kV Zeiss 10 CA transmission electron microscope, which is equipped with a Morada CCD camera, and analyzed using iTEM software and Image J. The average AuNP diameter and size distribution were determined on the basis of the analysis of >700 nanoparticles in the TEM images.

Dynamic Light Scattering (DLS) and ζ-Potential Measurements. Dynamic light scattering and ζ-potential measurements of PON−AuNPs were performed using a Malvern Zeta Sizer instrument. Samples were measured in triplicate using disposable plastic cuvettes. The ζ-potential measurements were performed in disposable Malvern Zeta cells (DTS1070).

UV−Vis Spectroscopy. UV−vis extinction spectra of AuNPs solutions were recorded using a Thermofisher Evolution 201 UV−vis spectrometer. Measuring the red shift of the AuNPs plasmonic peak, originally at λ_{max} = 525 nm, allows easy tracking of the conjugation of HEG and PONs to AuNPs. The AuNPs extinction was also measured at 450 and 600 nm to track any nanoparticle aggregation.[29] The concentration of AuNPs was determined using experimentally verified extinction coefficients for AuNPs, which were previously measured by Haiss et al.[29]

X-ray Photoelectron Spectroscopy (XPS). Au substrates were manufactured by sputtering a few hundred nanometers of gold onto a silicon chip (NIST, Gaithersburg). To remove adventitious carbon, substrates were sputter-cleaned with Ar^+ ions using a PHI 04-303 Differential Ion Gun in a PHI 5600 XPS system (Chanhassen, MN). Each substrate was removed from vacuum and directly placed into 300 μL of a 21.8 mM HEG spacer in 20 mL of reverse osmosis purified (RO) water in a 70 × 50 Kimax dish, capped with a glass Petri dish, and allowed to react overnight. Substrates were then rinsed at least 10× with RO water to wash away the excess unreacted HEG linker. The HEG−Au substrate was removed from the RO water Kimax dish with wafer forceps and placed on a Kimwipe to wick away water from the bottom of the substrate. It was then placed on the same sample stub on which it was sputtered with copper clips and was stored in a vacuum desiccator until introduction into the XPS ultra-high vacuum (UHV) chamber. To prepare PONs-50−Au and PONs-100−Au substrates, an HEG−Au substrate was placed into 20 mL of HEPES in a 70 × 50 Kimax dish and functionalized with 200 μL of 3.3 mM PONs-50 or PONs-100, 200 μL of 50 mM NHS, and 100 μL of 50 mM EDC. The substrate was capped with a glass Petri dish and allowed to react for 4 h. The reaction solution was then pipetted out, and the substrate was rinsed with ca. 10 mL of HEPES and then washed 10× with RO water. The PONs-50−Au and PONs-100−Au substrates were introduced into the UHV chamber in a similar manner to that for HEG−Au substrates, as described above. XPS was carried out with a Mg source (1253.6 eV) at 58.7 eV pass energy ($P_{base} = 10^{-9}$ Torr, 0.125 eV/step, 20 sweeps) on a PHI 5600 XPS system (Chanhassen, MN). Binding energy scales were calibrated using Au $4f_{7/2}$ = 84.00 eV. XPS peaks were fit with a Shirley baseline and analyzed using commercial software (CasaXPS Software). Two separate sets of "50% PONs Au" and "100% PONs Au" samples

DOI: 10.1021/acs.langmuir.7b04285
Langmuir 2018, 34, 4614−4625

Scheme 1. Synthesis of Poly(oxonorbornene)-Coated Gold Nanoparticles PONs−AuNPs[a]

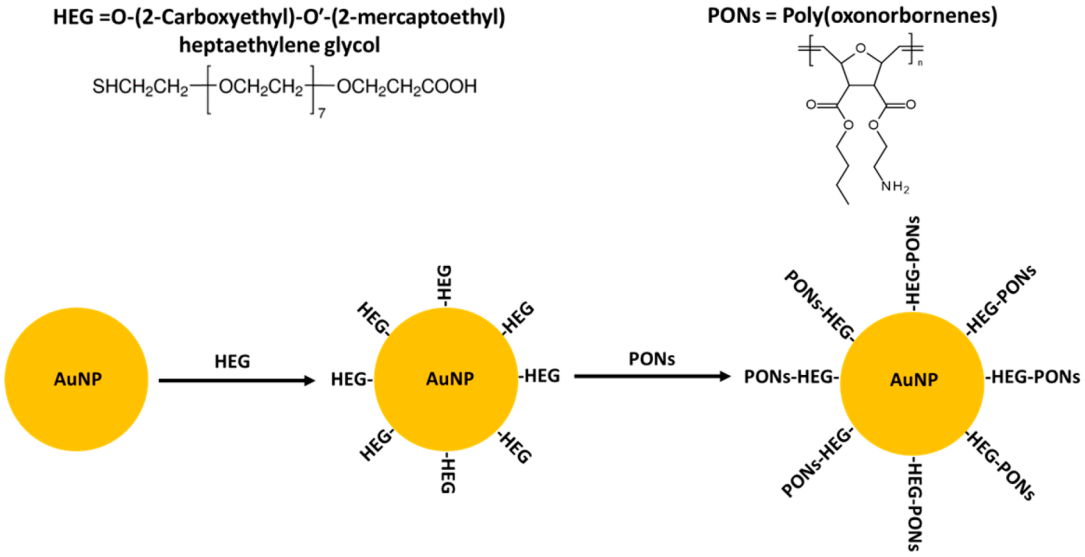

[a]Citrate-capped AuNPs are modified with HEG and then covalently modified with PONs using EDC coupling. The conjugation of PONs-50 to AuNPs is shown as an example. The schematic diagram is illustrative and not drawn to scale.

were generated on different days and yielded very similar XPS data, as judged by the ratio of the Au(4f) to N(1s) areas.

Thermogravimetric Analysis (TGA). Ahead of thermogravimetric analysis, PONs−AuNPs were centrifuged at 3000 RCF for 10 min at 25 °C and the supernatant was removed. The pelleted nanoparticles were transferred to a heating pan, which was placed into a PerkinElmer Pyris 1 thermogravimetric analysis instrument and heated for 15 min at 100 °C to remove water. The temperature was then increased by 25 °C/min until it reached 900 °C. The mass loss between 100 and 650 °C was used to determine the total amount of HEG and PONs originally on the nanoparticle surface.[30]

Fluorescamine Assays. Free PONs were used to construct calibration curves that describe the fluorescence intensity of fluorescamine−PONs conjugates as a function of PONs concentration. The fluorescamine assays were conducted in 5 mM sodium borate buffer solution at pH 8 in standard 1 mL cuvettes. Each sample contained PONs with 50% (PONs-50) or 100% (PONs-100) amine/ammonium content, at concentrations ranging from 0.2 to 2 μM. Fluorescamine in acetonitrile solution was added to each sample to achieve a final concentration of 1 mM. The solution was stirred briefly to ensure mixing. The reaction between PONs and fluorescamine was carried out at room temperature and monitored using steady-state fluorescence spectroscopy. Fluorescence spectra were recorded at an excitation wavelength of 425 nm until the fluorescence peak intensity at 480 nm was stabilized, typically at about 1 h from the beginning of the reaction. The fluorescence intensity at 480 nm was plotted against PON concentration to construct the calibration curves for PONs-50 and PONs-100 amine/ammonium content. Samples of PONs−AuNPs were analyzed for PONs content by first removing the PONs from AuNPs and then analyzing the level of released PONs using the fluorescamine assay as described above. Solutions (15 mL, 0.2 nM) of the PONs-50−AuNPs and PONs-100−AuNPs were washed via centrifugation at 6000 RCF for 15 min at 25 °C to remove excess PONs. The PON−AuNP pellets were resuspended in 1 mL of 10 mM HEPES buffer at pH 6.0. All PONs−AuNPs samples were diluted to give a UV−vis absorption of 0.24 OD at 450 nm to ensure that the AuNPs concentrations were the same for all samples. At 450 nm, the extinction coefficient of AuNPs is similar over a broad range of nanoparticle diameter and the absorption intensity is not affected by aggregation or by plasmonic peak shifts resulting from changes in the surface chemistry.[29] The solutions were then centrifuged for 15 min at 10 000 RCF and 25 °C, and the supernatant was removed. A 1.5 mL solution containing 25 mM sodium borohydride in pH 8 borate buffer was added to each sample, and the solution was incubated overnight to ensure that all PON molecules were removed from the surface of the AuNPs and that any excess sodium borohydride was hydrolyzed. The samples were centrifuged for 15 min at 20 000 RCF and 25 °C to remove the AuNPs, and the supernatants were analyzed for amine content by reacting them with fluorescamine and recording the resulting fluorescence spectra as described above for free PONs. The concentrations of PONs, which were released from the surface of the AuNPs, were calculated using the fluorescamine calibration curves constructed for free PONs.

Fluorescence Leakage Assays. Steady-state fluorescence measurements with an excitation wavelength of 480 nm were carried out using a PTI QuantaMaster 300. The test substances (PONs or PONs−AuNPs solutions) were added as 50 μL aliquots to final solution volumes of 2 mL of 10 mM HEPES buffer at pH 7.0 with concentrations ranging from 0.33 to 33 μM (PONs) and 0.015 to 0.24 nM (PONs−AuNPs). Free PONs samples were solubilized in DMSO and then added to the liposome solution. PONs−AuNPs samples were solubilized in 10 mM HEPES buffer at pH 7.0. The increasing fluorescence intensity due to liposome lysis was monitored at 515 nm until the fluorescence intensity stabilized typically after 10 min. Complete leakage was measured following the addition of 50 μL of 1% Triton X-100 in deionized water. All experiments were carried out at room temperature.

RESULTS AND DISCUSSION

Design of PONs−AuNPs. A schematic diagram illustrating the molecular structure of PONs and their covalent conjugation to AuNPs to form PONs−AuNPs is shown in Scheme 1. Depending on their butyl/amine ratio, PONs, which have been synthesized following a previously reported procedure,[17,19,24,25] ranged in their molecular weight between 3832 and 4702 g mol^{-1} (amine groups are protected with BOC) and had a polymer chain length of 10 repeat units. It should be noted that PONs with an amine/alkyl ratio of 1 (50% amine/ammonium content) have been reported in previous studies to have the highest antimicrobial activity.[17,24] PONs with this chain length and molecular weight are comparable to in length and molecular weight to peptides that were previously conjugated successfully to AuNPs using 1-ethyl-3-(3-dimethylaminopropyl)carbodiimide hydrochloride (EDC) cou-

DOI: 10.1021/acs.langmuir.7b04285
Langmuir 2018, 34, 4614−4625

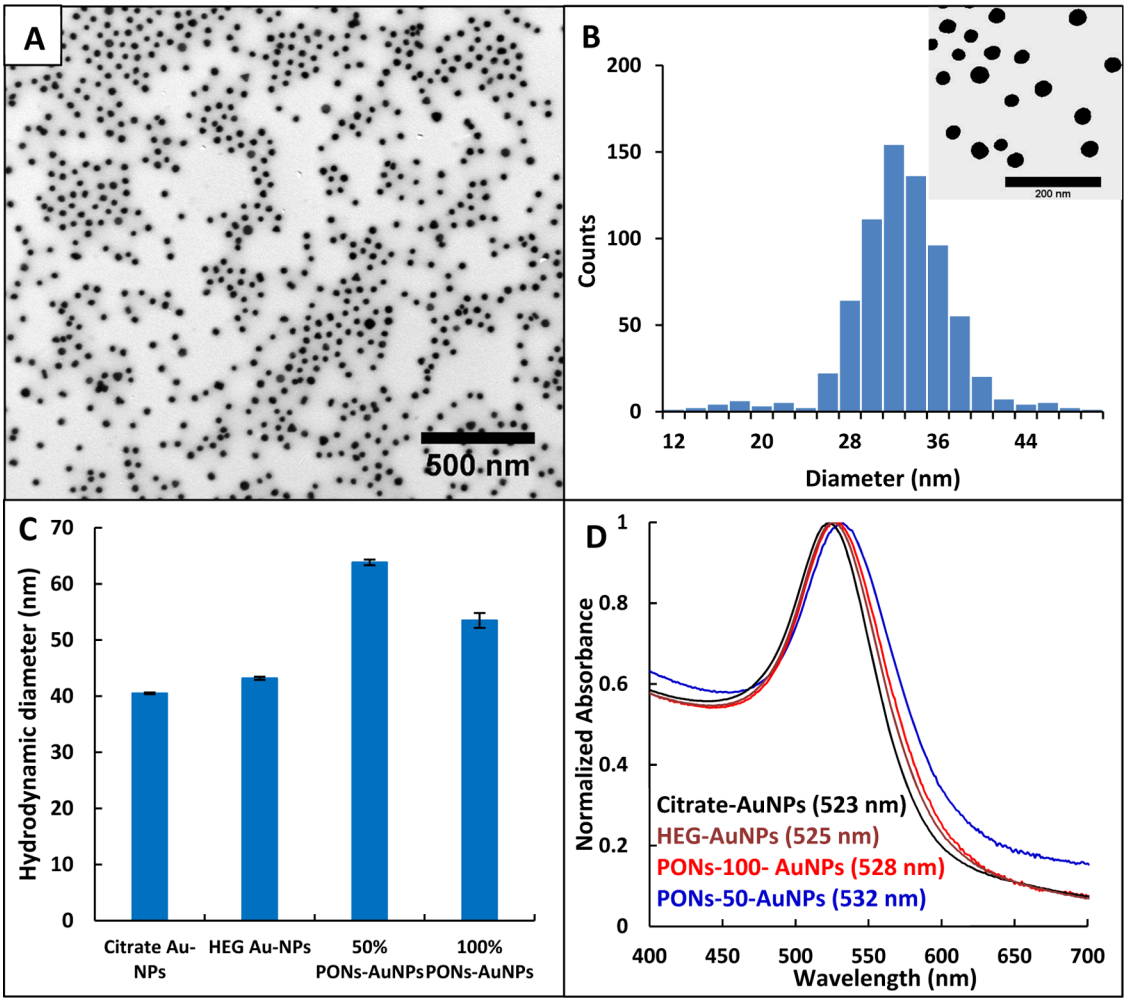

Figure 1. (A) Transmission electron microscopy (TEM) image of PONs-50−AuNPs at 31 500× (B) A histogram showing the average size and size distribution of >700 PONs-50−AuNPs to be 32 ± 4.6 nm. A zoomed-in image at 100 000× of the AuNPs is shown as insert. (C) Hydrodynamic diameter of functionalized AuNPs from dynamic light scattering (DLS) measurements: citrate-functionalized AuNPs (40.5 ± 0.2 nm), HEG−AuNPs (43.1 ± 0.3 nm), PONs-50−AuNPs (63.8 ± 0.5 nm), and PONs-100−AuNPs (53.5 ± 0.5 nm). (D) UV−vis absorption spectra of citrate−AuNPs (λ_{max} = 523 nm, black), HEG−AuNPs (λ_{max} = 525 nm, brown), PONs-50−AuNPs (λ_{max} = 532 nm, blue), and PONs-100−AuNPs (λ_{max} = 528 nm, red).

pling.[31] As shown in Scheme 1, AuNPs with an average diameter of 32 nm were synthesized in the presence of citrate; the AuNPs were then functionalized with HEG to form carboxyl-modified negatively charged AuNPs (ζ-potential of ∼−30 mV). EDC coupling was then used to conjugate the amine-rich PONs to the AuNPs (ζ-potential values ranging from +15 to +35 mV).

Characterization of PONs−AuNPs. Transmission electron microscopy (TEM), dynamic light scattering (DLS), and UV−vis extinction spectroscopy were used to determine the size, size distribution, morphology, and aggregation state of AuNPs and for real-time monitoring of the covalent conjugation of PONs to AuNPs. A representative TEM image of PONs-50−AuNPs at 31 500× is shown in Figure 1A. A histogram showing the size and size distribution of >700 PONs−AuNPs, shown in Figure 1B, indicates an average AuNP diameter of 32 ± 4.6 nm. A zoomed-in image of the PONs-50−AuNPs at 100 000× is shown as insert. The AuNPs appear to be approximately round and well-spaced even after drying onto the TEM grid, which is indicative of minimal or no aggregation. DLS data for citrate-coated AuNPs, HEG-modified AuNPs, PONs-50−AuNPs, and PONs-100−AuNPs are shown in Figure 1C. Citrate-capped AuNPs show an average hydrodynamic diameter of 40.5 ± 0.2 nm, which is larger than the value determined for AuNPs by TEM. The difference between the AuNPs diameter obtained by TEM and their hydrodynamic diameter obtained by DLS is partially because the contribution of the low-electron-density PONs coating to the diameter of AuNPs is not seen in the TEM images. Additionally, our DLS measurements were taken at a single angle (175°). Precise measurements to obtain the true hydrodynamic diameter would require DLS measurements at various wavelengths and concentrations (c) and extrapolation to 0° and c = 0 g mol^{-1} (dynamic Zimm plot).[33] However, this was not possible with our setup and is also not needed because only relative changes in the diameter of AuNPs due to PONs conjugation were sought. The hydrodynamic diameter of AuNPs slightly increased to 43.1 ± 0.3 nm following their functionalization with HEG. It further increased to 63.8 ± 0.5 and 53.5 ± 0.5 nm, respectively, following the covalent conjugation of PONs-50 or PONs-100 to the AuNPs. This corresponds to a PONs shell thickness of about 10 nm for PONs-50 and about 5 nm for PONs-100. The UV−vis extinction of AuNPs at their plasmon peak wavelength depends on the AuNP size and the dielectric

DOI: 10.1021/acs.langmuir.7b04285
Langmuir 2018, 34, 4614−4625

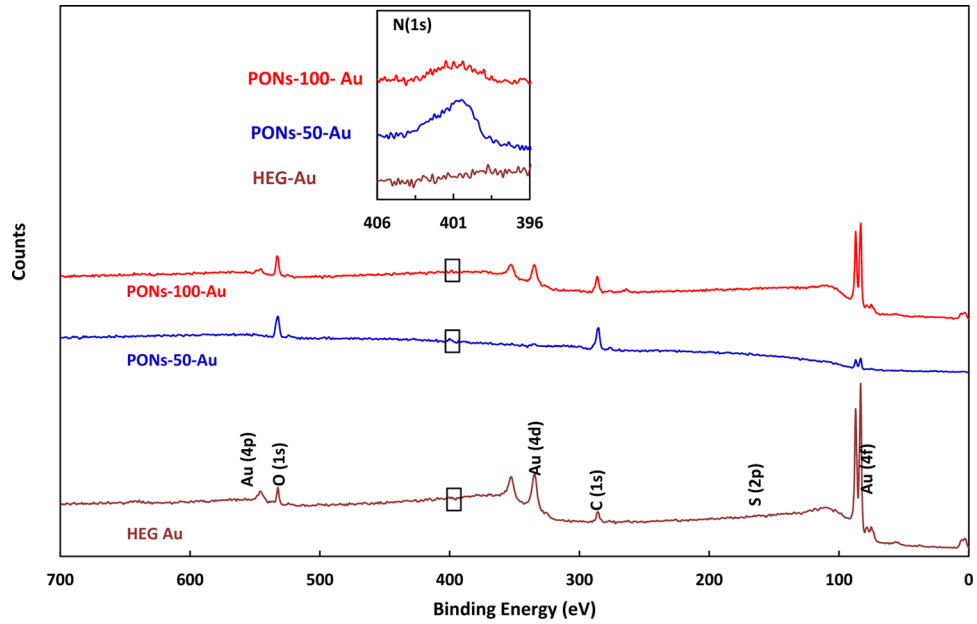

Figure 2. XPS spectra of gold substrates after functionalization with HEG (brown), PONs-50 (blue), and PONs-100 (red) with the N(1s) envelope shown in the insert.

constant of the nanoparticles' environment.[32] Conjugating molecules to the surface of AuNPs causes the plasmon peak to shift toward longer wavelengths, and the magnitude of that red shift is used to monitor the conjugation process. The UV−vis spectra of citrate-coated AuNPs, HEG-modified AuNPs, PONs-50−AuNPs, and PONs-100−AuNPs are shown in Figure 1D. The extinction peak maximum shifted slightly from 523 to 525 nm when AuNPs were modified with the HEG spacer. A more significant red shift to 532 nm was observed following the covalent conjugation of PONs-50 to the AuNPs. A smaller red shift to only 528 nm was obtained when PONs-100 molecules were conjugated to AuNPs, suggesting the formation of a thinner polymer coating with that polymer. The absorption peak widths remained largely unchanged throughout the polymer conjugation process, which indicates that the PONs−AuNPs did not aggregate. Aggregation of AuNPs would result in absorption peak broadening and the appearance of measurable absorption at 450 and 600 nm.[29]

X-ray Photoelectron Spectroscopy (XPS) of PONs−Au Substrates. Initial XPS experiments on AuNPs were complicated by the presence of large sulfur and nitrogen signals, attributed to excess HEPES buffer, which remained even after repeated centrifugation and rinsing with water, as well as large O(1s), Si(2p), and Si(2s) signals from the SiO_2 substrate onto which the nanoparticles were drop-cast. For these reasons, we decided to use a flat gold substrate as a surrogate for the AuNP surface. A similar approach was previously pursued by Ceccone and co-workers who utilized XPS to characterize the surface chemistry of gold substrates before and after functionalization with thiol-modified glucose self-assembled monolayers[34] and by Hamers and co-workers who employed XPS to determine the density of molecular ligands on AuNPs using flat Au substrates as a model system.[35] Flat gold substrates have several advantages over AuNPs: atomically clean surfaces can be generated prior to covalent attachment of adsorbates by sputter-cleaning, unwanted substrate signals are removed, and the flat surfaces are more easily washed and rinsed clean of species present in the solution (e.g., buffers) as compared with the AuNPs that must be repeatedly centrifuged and still retain traces of solution species. We hypothesized that the surface chemistry of flat Au substrates will be similar to that of the surface of the relatively large ∼30 nm AuNPs, which have relatively low curvature. This hypothesis was borne out by the experimental results, which were both reproducible and characterized by XPS data that are dominated by peaks associated with carbon, oxygen, and the gold substrate, consistent with the presence of only the HEG linker and PONs. The XPS spectra of HEG−Au (brown), PONs-50−Au (blue), and PONs-100−Au (red) substrates are shown in Figure 2. Evidence for the addition of the HEG spacer to Au is provided by the appearance of C(1s) and O(1s) peaks. The most striking feature of Figure 2, however, is that the Au(4f) peaks are much more significantly attenuated upon subsequent coupling of PONs-50 as compared to that with the PONs-100 molecules. As shown in the insert in Figure 2, the attachment of the PONs-50 molecules also leads to a measurably larger N(1s) signal intensity than that in PONs-100 conjugation, even though PONs-100 molecules contain twice as many nitrogen atoms as PONs-50 molecules. Thus, results from the Au(4f) and N(1s) regions point toward a greater surface coverage of PONs-50 molecules. By using the integrated area of the N(1s) peaks as a relative measure of the PONs coverage and accounting for the greater nitrogen content in the PONs-100 molecules, the surface coverage of PONs-50 molecules is about 4.5 times greater than that of the PONs-100 molecules. This estimate of the relative coverage is also qualitatively consistent with the decrease in the Au(4f) peak area, which decreases by 95% upon coupling of PONs-50 and by 23% upon coupling of PONs-100 molecules. It should be noted that although XPS analysis of the AuNPs was complicated by the presence of contaminants from the solution and unwanted substrate peaks, a significantly lower Au(4f) peak was observed upon coupling of PONs-50 as opposed to that of PONs-100 molecules to AuNPs, in qualitative agreement with the results presented here for PONs coupling to flat Au substrates.

DOI: 10.1021/acs.langmuir.7b04285
Langmuir 2018, 34, 4614−4625

Thus, the UV−vis, DLS, and XPS results all indicate that the surface coverage of PONs depends on their molecular structure, with a greater surface coverage of the PONs-50. To confirm this observation, we desorbed the PONs from the AuNPs into the solution and determined the released amount of PONs by employing thermogravimetric analysis (TGA, thermal desorption) and fluorescamine assays (chemically induced desorption).

Thermogravimetric Analysis of PONs−AuNPs. Thermogravimetric analysis (TGA) measurements were used to estimate the amount of organic content in PONs−AuNPs with varying amine content. TGA spectra of HEG−AuNPs (brown), PONs-50−AuNPs (blue), and PONs-100−AuNPs (red) between 100 and 900 °C are shown in Figure 3. Mass losses

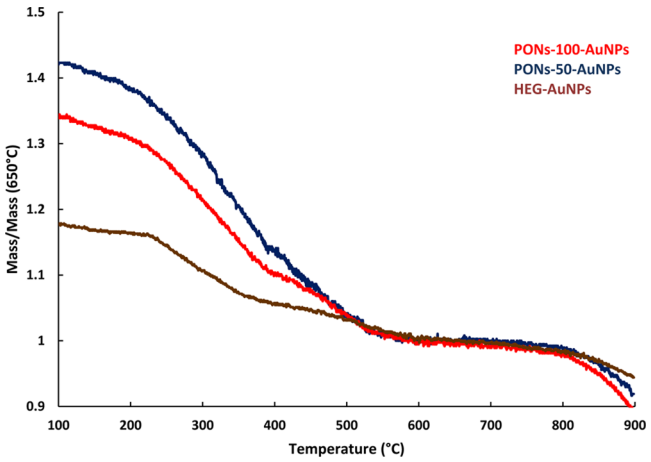

Figure 3. Thermogravimetric analysis (TGA) traces of HEG (8)-carboxyl-functionalized gold nanoparticles (HEG−AuNPs) (brown), PONs-50−AuNPs (blue), and PONs-100−AuNPs (red). The mass values are normalized to the mass value at 650 °C, a temperature where all organic content is desorbed from the AuNPs surface.

from the HEG−AuNPs and PONs−AuNPs were normalized to the remaining mass at 650 °C, where all organic content is assumed gone from the AuNPs surface. The mass losses were 18 ± 2% for HEG−AuNPs, 43 ± 3% for PONs-50−AuNPs, and only 34 ± 3% for PONs-100−AuNPs. Subtracting the mass fraction of the HEG spacer, the PONs-50 relative content on PONs-50−AuNPs was about 25%, whereas the relative content of PONs-100 on PONs-100−AuNPs was only 16%. Within the error, this result is consistent with the DLS and UV−vis results, which indicate a significantly higher polymer coverage when AuNPs are coated with PONs-50 compared to when coated with PONs-100 molecules.

Fluorescamine Assays of PONs Released from PONs−AuNPs. AuNPs solutions were treated with sodium borohydride to reduce the thiol bonds and release the organic (surface) content from the AuNPs into the solution. Representative fluorescence spectra (excitation wavelength, λ_{ex} = 425 nm) of solutions containing 1 mM fluorescamine and free PONs-50 or PONs-100, respectively, at concentrations varying from 0.2 to 2 μM are shown in Figure 4A (PONs-50) and Figure 4B (PONs-100). Calibration curves describing the concentration-dependent fluorescence intensity at 480 nm (peak intensity) for PONs-50 (Figure 4C) and PONs-100 (Figure 4D) show linear fits with a R^2 value of 0.998 for PONs-50 and 0.996 for PONs-100 in a concentration range between 0 and 1.6 μM. Fluorescence peak intensities were measured in triplicate (the error bars are typically smaller than the data point size in the figure). To determine the PONs content of PONs−AuNPs, samples of PONs-50−AuNPs, and PONs-100−AuNPs with identical AuNPs concentrations (determined by UV−vis measurements) were added to 10 mL solutions containing 25 mM sodium borohydride in a 50 mM borate buffer (pH 8.0). The PONs−AuNPs solutions were incubated overnight at room temperature to ensure that all conjugated PONs were released from the AuNPs following the reduction of surface thiol bonds. AuNPs were then removed from the solutions by centrifugation at 20 000 RCF for 15 min at 25 °C, and sample supernatants were assayed for their amine content using the fluorescamine assay. Control experiments were carried out to confirm that incubating fluorescamine with hydrolyzed sodium borohydride solutions does not lead to a significant change in the fluorescence signal. The supernatant solutions were diluted in borate buffer (pH 8.0) by the same dilution factor for PONs-50 and PONs-100 to realize polymer concentrations similar within the range of PONs concentrations used to construct the calibration curves. The fluorescamine assays revealed that the concentrations of released PONs were 1.7 μM PONs-50, just outside the linear range of the calibration curve for PONs-50, and 0.5 μM PONs-100.

ζ-Potential Measurements of PONs−AuNPs. Realizing that the molecular structure of PONs affects their surface coverage on AuNPs, we conducted ζ-potential measurements to determine the cationic charge density of PONs−AuNPs as a function of the amine/ammonium content of PONs (see Figure 5). To enable these measurements, we conjugated PONs with varying amine/ammonium content (50, 55, 75, 95, and 100%) to HEG−AuNPs following the same EDC covalent conjugation strategy (see Experimental Methods for details). Prior to the covalent attachment of the PONs to AuNPs, the carboxyl-terminated HEG-coated AuNPs had a negative ζ-potential of −32 ± 3 mV. As expected, the ζ-potential values of PONs−AuNPs with varying amine/ammonium content were all positive, confirming the presence of primary ammonium groups of PONs on the AuNP surface. The highest ζ-potential (37 ± 7 mV) was measured for PONs-50−AuNPs. A further increase of the amine/ammonium content of free PONs lowered the ζ-potential to +25 ± 9 mV for PONs-55−AuNPs and to +15 ± 7 mV for PONs-75−AuNPs. The ζ-potential remained the same at +15 ± 7 mV for PONs-95−AuNPs and +17 ± 13 mV for PONs-100−AuNPs. The same qualitative trend was found when PONs were previously conjugated to flat surfaces although with overall lower impact.[20] The highest ζ-potential values were measured for the polymers with the lowest nominal ammonium/amine content, and a minimum was obtained for PONs-95.[20] The decrease in ζ-potential of PONs−AuNPs with the increasing ammonium/amine content of PONs is consistent with the lower polymer coverage of PONs with the increasing amine content on AuNPs. It is also possible that increasing the amine content of PONs results in lower degree of amine protonation. A decrease in the degree of protonation in amine-containing polymers with increasing amine density was previously reported in molecular modeling studies.[36] These calculations are consistent with polyelectrolyte theory, which stipulates a minimum distance (Bjerrum length) between amine groups for them to remain protonated.[37] According to the modeling study, the decreased distance between the amine groups, below the Bjerrum length, in PONs with ammonium content over 50% would lower the degree of

DOI: 10.1021/acs.langmuir.7b04285
Langmuir 2018, 34, 4614−4625

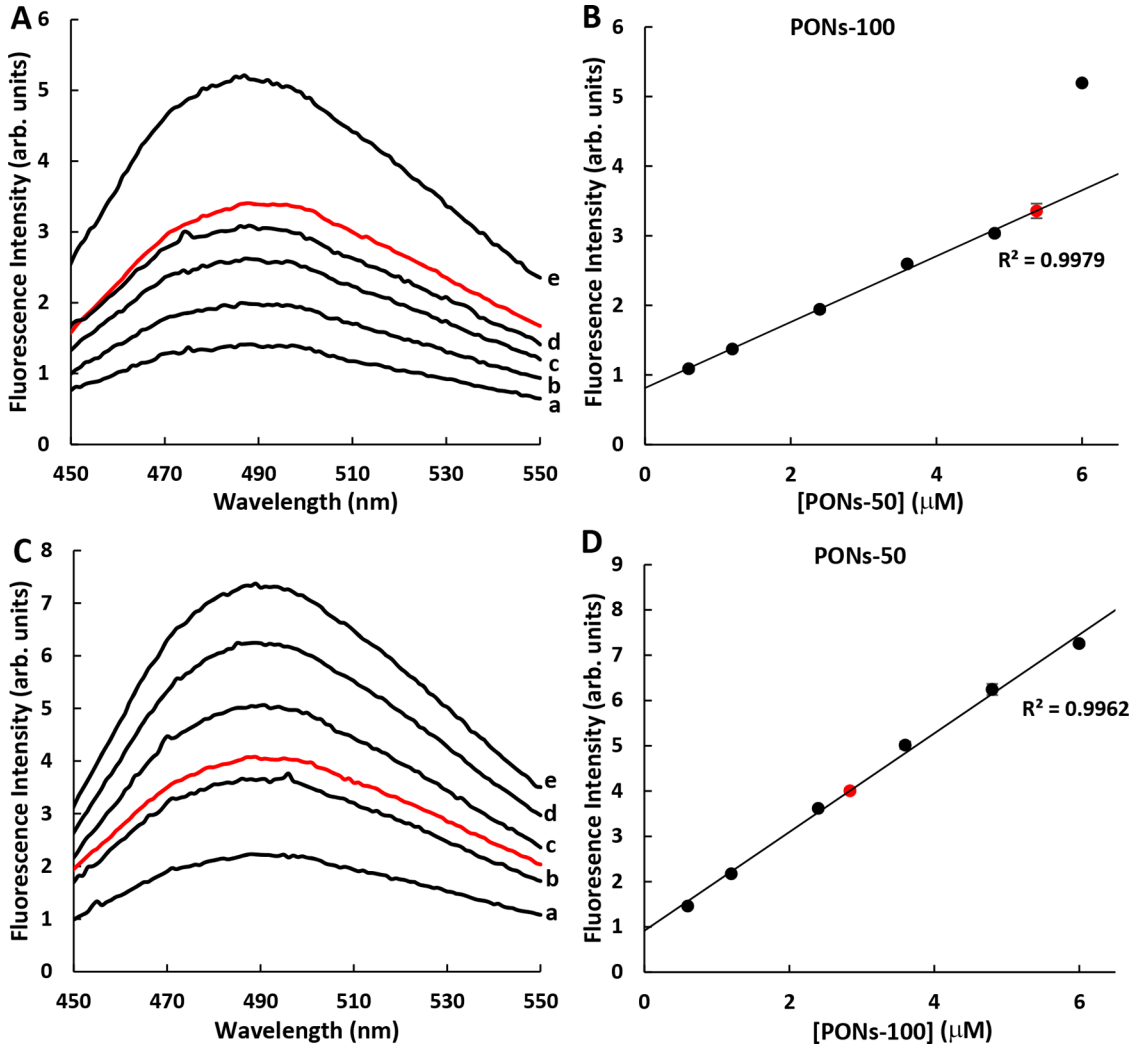

Figure 4. Fluorescamine assays of free PONs and PONs–AuNPs: (A) PONs-50 (black) and PONs-50–AuNPs (red); (B) PONs-100 (black) and PONs-100–AuNPs (red). The fluorescamine emission increases (C and D) with increasing PONs concentrations of (a) 0.4 μM, (b) 0.8 μM, (c) 1.2 μM, (d) 1.6 μM, and (e) 2.0 μM.

amine protonation and the overall charge density. However, although a significant decrease in the ζ-potential of PONs–AuNPs is observed when the amine/ammonium content of PONs increases from 50 to 75%, the fact that the ζ-potential values remain largely constant when the amine/ammonium content of PONs increases further from 75 to 100% suggests that intramolecular interactions between adjacent amines in PONs are not the only and perhaps not the most important interactions in PONs–AuNPs and that the PONs coverage and morphology have a greater effect on the PONs–AuNPs ζ-potential and membrane activity as shown in the next section.

Together, the smaller hydrodynamic diameter (DLS, Figure 1C), the smaller plasmonic peak shift in the UV–vis spectrum (UV–vis, Figure 1D), the higher Au(4f) and smaller N(1s) peaks in the XPS spectra (Figure 2), the lower amine content obtained with the TGA measurements (Figure 3) and fluorescamine assays (Figure 4), and the decreasing ζ-potential (Figure 5), as the amine content in PONs that are covalently attached to AuNPs increases, clearly prove that the molecular structures of PONs strongly impact the conjugation efficiency of PONs to the AuNPs surface. This results in a significantly lower polymer surface coverage and amine/ammonium density, as the hydrophilicity of PONs increases. Scheme 2 illustrates this impact. PONs-50 molecules are bound to the surface through a covalent attachment at a single position, and the polymer chains largely point out into the solution. This leads to a maximum coverage and high hydrodynamic diameter. In contrast, covalent attachment of PONs-100 to AuNPs leads to a positive charge buildup on the surface, which inhibits the covalent attachment of additional PONs-100 molecules because of repulsive electrostatic interactions. The absence of alkyl groups in PONs-100 enables binding of PONs-100 to the AuNPs surface via multiple amines, which further blocks additional surface binding sites. This has a negative impact on the order of the PONs assemblies and significantly reduces the polymer coverage and thickness on the AuNPs surface.

Membrane Activity of PONs and PONs–AuNPs Studied Using Fluorescence-Based Liposome Lysis Assays. Fluorescence-based liposome lysis assays were carried out to determine the impact of free PONs and PONs–AuNPs with varying amine/ammonium content on negatively charged calcein-containing POPC/POPG liposomes. The fluorescence emission from calcein-containing liposomes at 515 nm (λ_{ex} = 480 nm) is initially weak due to fluorescence self-quenching of the highly concentrated calcein molecules inside the liposomes. When these liposomes interact with membrane-active sub-

DOI: 10.1021/acs.langmuir.7b04285
Langmuir 2018, 34, 4614–4625

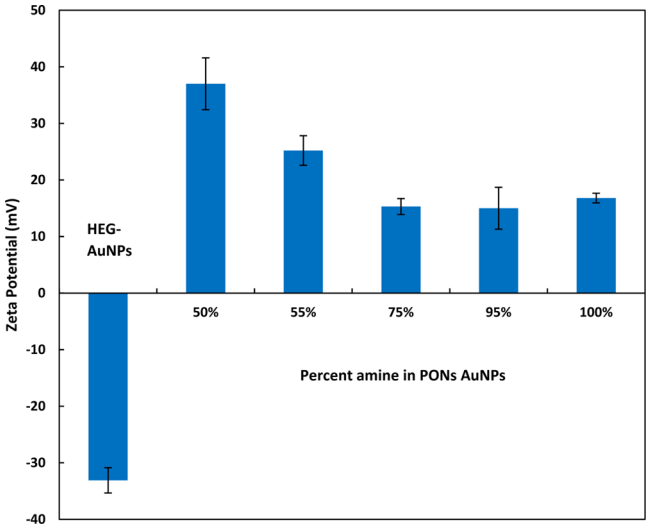

Figure 5. ζ-Potential of HEG–AuNPs (negatively charged) and PONs–AuNPs with increasing amine content from 50% (1:1 amine/butyl ratio) to 100% (PONs were synthesized from diamine oxonorbornene monomers). ζ-Potential values were measured in triplicate, and the error bars represent the range of measured values.

stances, the fluorescence intensity of the solution increases because of membrane disruption, which enables calcein leakage to the solution and dilution. Figures 6A,C show the time-dependent fluorescence intensity of calcein-containing liposomes when incubated with PONs-50 at increasing concentrations ranging from 0.33 to 33 μM (Figure 6A) and of PONs-50–AuNPs at increasing concentrations ranging from 0.015 to 0.24 nM (AuNPs concentrations, Figure 6C). Figures 6B,D show the concentration dependence of the lysis efficiencies (%) of PONs-50 (Figure 6B) and PONs-50–AuNPs (Figure 6D). Prior to adding a sample of free PONs or PONs–AuNPs, only background fluorescence is observed. A fluorescence increase is observed because of membrane disruption when PONs or PONs–AuNPs samples are added to the solution. The fluorescence intensity stabilizes as the liposome solution reaches equilibrium. Then, 50 μL of 1% aqueous Triton X-100 is added to fully rupture the liposomes and obtain maximum fluorescence. The ratio $[(I_{max} - I_c)/(I_{max} - I_b)] \times 100$, where I_{max} is the final and maximum fluorescence intensity when the liposomes are all lysed, I_c is the equilibrium fluorescence intensity when the liposomes are exposed to PONs or PONs–AuNPs samples at a given concentration, and I_b is the background fluorescence, is used to calculate the percent lysis of the liposomes. The concentration range of the AuNPs is limited because at concentrations higher than 0.24 nM, the AuNPs have a significant extinction at 480 nm, which induces an inner filter effect. Using the lysis plots in Figure 6, the concentration of PONs-50 needed to cause 50% liposome

Scheme 2. The Impact of PONs Amine/Alkyl Ratio on their Binding to AuNPs[a]

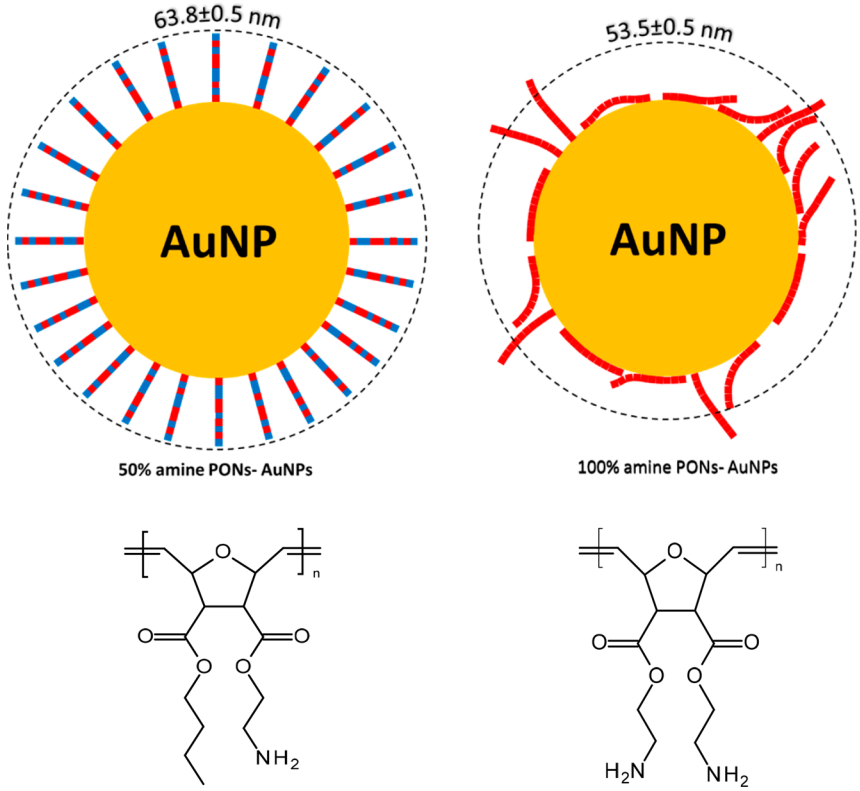

[a]Dynamic light scattering (DLS), UV–vis spectroscopy, XPS, thermogravimetric analysis (TGA) measurements, fluorescamine assays, and ζ-potential measurements strongly suggest that PONs-50 molecules (amine/butyl ratio of 1 defined as 50% amine content) are covalently conjugated to AuNPs via single-point attachment. This maximizes PONs-50 surface coverage on AuNPs (left). In contrast, because of higher hydrophilicity, PONs-100 molecules (made from diamine monomers, defined as 100% amine content) are not as surface-active. Fewer PONs-100 molecules bind to the surface, and they attach to AuNPs via multiple amines, which blocks surface binding sites (right). This results in significantly reduced polymer coverage and a disorganized thin PONs coating with limited amine/ammonium groups that are available to interact with liposomes.

DOI: 10.1021/acs.langmuir.7b04285
Langmuir 2018, 34, 4614–4625

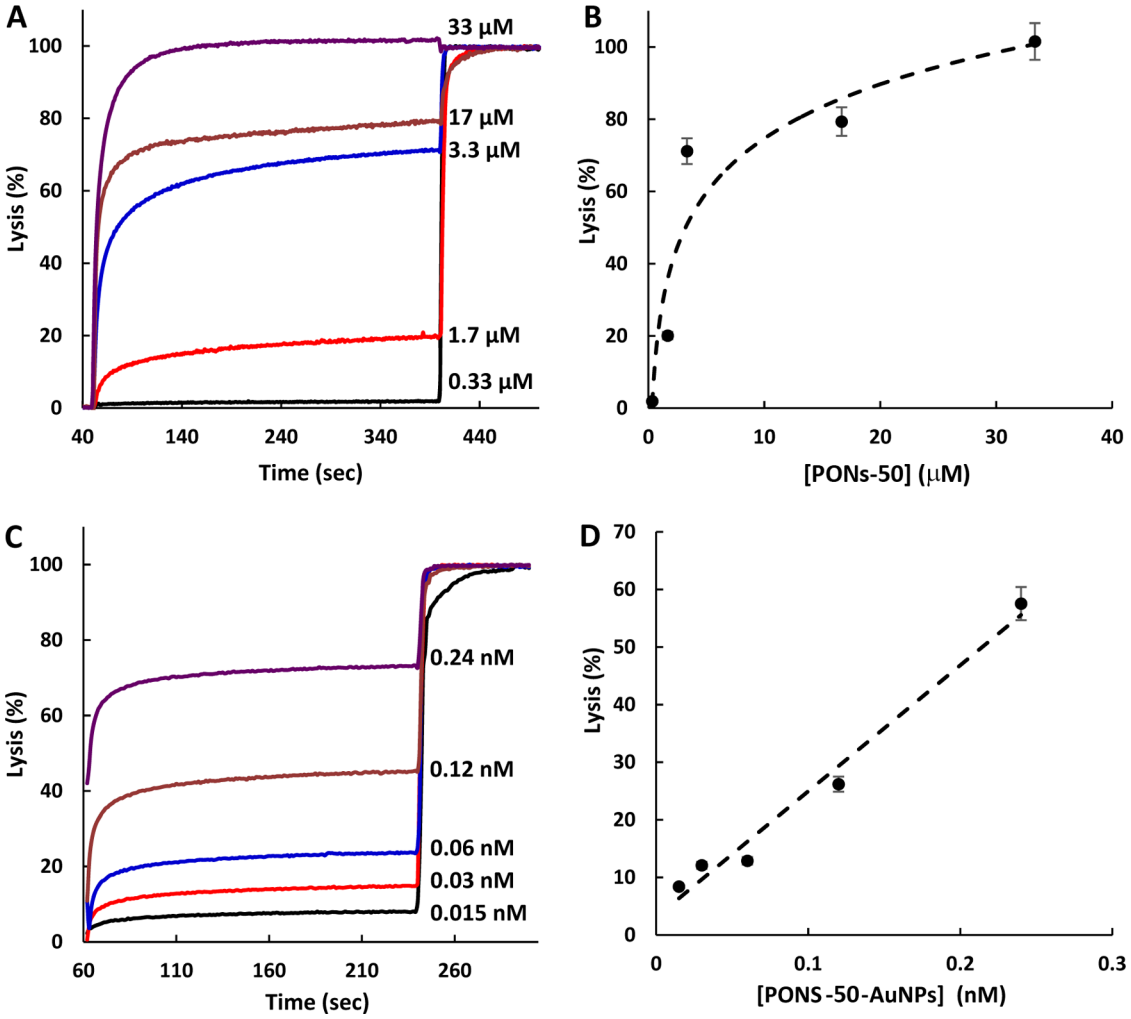

Figure 6. . Time-dependent fluorescence intensity of calcein-containing liposomes when incubated (A) with PONs-50 at concentrations ranging from 0.33 to 33 μM and (C) with PONs-50−AuNPs at AuNPs concentrations ranging from 0.015 to 0.24 nM. (B and D) Percent lysis as a function of PONs-50 and PONs-50−AuNPs concentration, respectively. The percent lysis values were measured in triplicate. The error bars indicate the range of percent lysis values obtained for each exposure.

lysis was 1.1 μM, whereas the concentration of PONs-50−AuNPs required to cause 50% liposome lysis was 0.15 nM. On the basis of the fluorescamine assay results, each AuNP is coated with approximately 1000 PONs-50 molecules. At 0.15 nM PONs-50−AuNPs, the equivalent PONs concentration is 0.15 μM, about 10 times lower than the concentration of free PONs-50 required for 50% liposome lysis. The 10-fold increase in membrane activity of PONs-50−AuNPs compared to that of free PONs-50 under these conditions is likely due to the high local concentration of ammonium ions at the point of contact between PONs-50−AuNPs and the liposome membranes. This finding is consistent with previous studies that investigated the impact of PAH-coated AuNPs on liposomes and living organisms.[5] However, as described in the following section, our studies reveal a more nuanced picture of the interactions between PONs−AuNPs and phospholipid membranes.

Now that we know that the molecular structure of PONs affects the surface coverage, polymer thickness, and morphology of PONs on PONs−AuNPs, we determined the impact of the amine content of PONs on the membrane disruption activity of PONs−AuNPs. Figure 7 describes the liposome lysis efficiency (%) of free PONs (blue) and PONs−AuNPs (purple) with varying amine content. The concentrations of PONs (3.3 μM) and PONs−AuNPs (0.24 nM NP) were selected because the lysis efficiency was maximized at these PONs and PONs−AuNPs concentrations. For free PONs, the liposome lysis efficiency increases with the increasing amine content of up to 75%. A further increase in the amine content to 95 and 100% (fully diamine polymer) results in a sharp reduction in the liposome lysis efficiency, which is indicative of weaker interactions between free PONs with decreasing hydrophobicity and phospholipid membranes. For PONs−AuNPs, the liposome lysis efficiency is maximized for PONs-50−AuNPs. A further increase in the amine/ammonium content of PONs leads to a significant reduction in the liposome lysis efficiency down to under 5%, which is attributed primarily to the lower polymer coverage on the surface of AuNPs. Generally, the lysis efficiency of PONs−AuNPs is correlated with the measured ζ-potential of the nanoparticles, shown in Figure 5. PONs-50−AuNPs showed the highest ζ-potential and liposome lysis efficiency, whereas the PONs-95−AuNPs and PONs-100−AuNPs had lower ζ-potentials and lysis efficiencies. Interestingly, surface-attached polymer networks made from these PONs had almost identical ζ-potentials in the pH range of 6.5−8.0.[21] As these networks had complete surface coverage (as demonstrated by atomic force microscopy), the ζ-

DOI: 10.1021/acs.langmuir.7b04285
Langmuir 2018, 34, 4614−4625

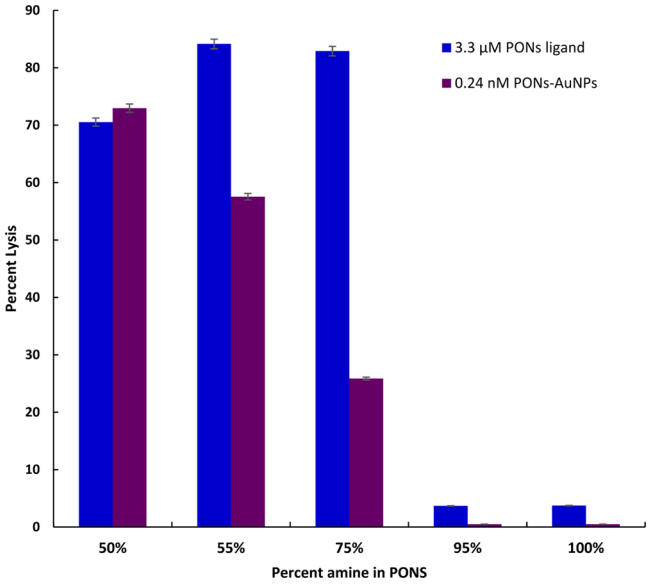

Figure 7. Percent lysis efficiency of liposomes incubated with free PONs (blue) and PONs–AuNPs (purple). Percent lysis values were measured in triplicate, and the error bars represent the range of values for each exposure. PONs–AuNPs with 95 and 100% amine content show lysis efficiencies lower than 1% that could not be distinguished from background noise.

potential differences of the PONs–AuNPs are consistent with the differences in PONs surface coverage on AuNPs.

SUMMARY AND CONCLUSIONS

In this study, we used PONs as a model polymeric ligand for nanoparticle modification where the total amine character and ζ-potential could be tuned systematically. The tunability allowed us to probe how the amine content of PONs impacts the polymer surface coverage and characteristics of PONs–AuNPs, as well as the strength of interactions with model membrane systems and their membrane disruption activity. TEM, DLS, UV–vis, XPS, TGA, and flurescamine assays used to characterize the PONs–AuNPs revealed that overly packing amine groups in free PONs decreases the polymer surface coverage, possibly because the hydrophilic PONs-100 molecules are less surface-active than PONs-50 molecules. It is also possible that due to the higher amine density and lower binding efficiency, PONs-100 molecules are conjugated to the surface via multiple amines, which blocks the surface for further incoming PONs molecules. Therefore, high-amine-density PONs lead to a decrease rather than an increase in the PONs–AuNPs surface coverage, amine charge density, and availability to interact with phospholipid membranes. Under conditions where the surface coverage of PONs-50 is maximized, the membrane disruption activity of PONs-50–AuNPs is about 10-fold higher than that of free PONs-50. This is attributed to the increased local concentration of the membrane-active PONs-50 when PONs-50–AuNPs bound to phospholipid membranes. However, a further increase in the amine density of PONs results in a significant decrease in the membrane disruption activity of PONs–AuNPs. The study highlights the importance of surface coverage when comparing the activity of nanoparticle conjugates. It shows that even a slight change in the molecular structure can have a significant effect on the surface coverage and activity, in this case membrane disruption activity. The study also highlights the need to develop new and improved surface analysis techniques to quantitatively determine the surface coverage and orientation of ligands and polymer molecules on nanoparticle surfaces. The results of this study may have significant implications on applications that require conjugating amine-containing molecular ligands and/or polymers to the surface of nanoparticles. Clearly, the membrane activity of such functionalized nanoparticles does not necessarily scale linearly with the nominal number of amine groups on the target molecules. Rather, overly crowding amine-based drug molecules, enzymes, and antibodies on nanoparticles could lead to changes in the surface coverage of the nanoparticles that would decrease rather than increase the activity of the nanoparticle conjugates. It is therefore imperative to optimize the surface coverage of such conjugates on the nanoparticle surface to maximize their activity.

ASSOCIATED CONTENT

Supporting Information

The Supporting Information is available free of charge on the ACS Publications website at DOI: 10.1021/acs.langmuir.7b04285.

PONs synthesis and ^{1}H characterization, PONs copolymerization scheme (Scheme S1), PONs copolymers characterization (Table S1), ^{1}H NMR spectra of Boc-protected PONs copolymers (Figure S1) and deprotected PONs copolymers (Figure S2), and GPC data of PONs copolymers (Figure S3) (PDF)

AUTHOR INFORMATION

ORCID

Tian A. Qiu: 0000-0002-7254-9233
Miranda J. Gallagher: 0000-0003-1139-1257
D. Howard Fairbrother: 0000-0003-4405-9728
Christy L. Haynes: 0000-0002-5420-5867
Karen Lienkamp: 0000-0001-6868-3707
Zeev Rosenzweig: 0000-0001-6098-3932

Notes

The authors declare no competing financial interest.

ACKNOWLEDGMENTS

This work was supported primarily by the National Science Foundation Center for Chemical Innovation (CCI) program Award CHE-1503408 for the Center for Sustainable Nanotechnology to Z.R., C.L.H., and D.H.F., and by the German Research Foundation Emmy-Noether grant LI1714/5-1 to K.L. A supplemental fellowship support for Z.Z.'s graduate assistantship was provided by the UMBC Chemistry Biology Interface program, which is supported by an NIH training grant: NIH-T32-GM066706.

REFERENCES

(1) Alkilany, A. M.; Murphy, C. J. Toxicity and Cellular Uptake of Gold Nanoparticles: What We Have Learned so Far? *J. Nanopart. Res.* **2010**, *12*, 2313–2333.

(2) Zhao, E.; Zhao, Z.; Wang, J.; Yang, C.; Chen, C.; Gao, L.; Feng, Q.; Hou, W.; Gao, M.; Zhang, Q. Surface Engineering of Gold Nanoparticles for in Vitro siRNA Delivery. *Nanoscale* **2012**, *4*, 5102.

(3) Qiu, Y.; Liu, Y.; Wang, L.; Xu, L.; Bai, R.; Ji, Y.; Wu, X.; Zhao, Y.; Li, Y.; Chen, C. Surface Chemistry and Aspect Ratio Mediated Cellular Uptake of Au Nanorods. *Biomaterials* **2010**, *31*, 7606–7619.

(4) Tarantola, M.; Pietuch, A.; Schneider, D.; Rother, J.; Sunnick, E.; Rosman, C.; Pierrat, S.; Sonnichsen, C.; Wegener, J.; Janshoff, A.

DOI: 10.1021/acs.langmuir.7b04285
Langmuir 2018, 34, 4614–4625

Toxicity of Gold-Nanoparticles: Synergistic Effects of Shape and Surface Functionalization on Micromotility of Epithelial Cells. *Nanotoxicology* **2011**, *5*, 254−268.
(5) Bozich, J. S.; Lohse, S. E.; Torelli, M. D.; Murphy, C. J.; Hamers, R. J.; Klaper, R. D. Surface Chemistry, Charge and Ligand Type Impact the Toxicity of Gold Nanoparticles to *Daphnia magna*. *Environ. Sci.: Nano* **2014**, *1*, 260.
(6) Tirrell, D. A.; Boyd, P. M. Interaction of Synthetic Polymers with Cell Membranes and Model Membrane Systems, 1. Differential Scanning Calorimetry. *Makromol. Chem., Rapid Commun.* **1981**, *2*, 193−198.
(7) Tirrell, D. A.; Turek, A. B.; Wilkinson, D. A.; McIntosh, T. J. Observation of an Interdigitated Gel Phase in Dipalmitoylphosphatidylglycerol Bilayers Treated with Ionene-6,6. *Macromolecules* **1985**, *18*, 1512−1513.
(8) Takigawa, D. Y.; Tirrell, D. A. Interactions of Synthetic Polymers with Cell Membranes and Model Membrane Systems. Part 6. Disruption of Phospholipid Packing by Branched Poly(ethylenimine) Derivatives. *Macromolecules* **1985**, *18*, 338−342.
(9) Seki, K.; Tirrell, D. A. pH-Dependent Complexation of Poly(acrylic Acid) Derivatives with Phospholipid Vesicle Membranes. *Macromolecules* **1984**, *17*, 1692−1698.
(10) Marwaha, L. K.; Tirrell, D. A. Interaction of Synthetic Polymers with Cell Membranes and Model Membrane Systems: Pyran Copolymer. *ACS Symp. Ser.* **1982**, 163−175.
(11) Takigawa, D. Y.; Tirrell, D. A. Interactions of Synthetic Polymers with Cell Membranes and Model Membrane Systems, 9. Reversal of Mg2+ Induced Structural Changes in Dipalmitoylphosphatidylglycerol Bilayers by Adsorbed Poly(ethyleneimine)s. *Makromol. Chem., Rapid Commun.* **1985**, *6*, 653−657.
(12) Kugler, R.; Bouloussa, O.; Rondelez, F. Evidence of a Charge-Density Threshold for Optimum Efficiency of Biocidal Cationic Surfaces. *Microbiology* **2005**, *151*, 1341−1348.
(13) Ikeda, T.; Tazuke, S.; Watanabe, M. Interaction of Biologically Active Molecules with Phospholipid Membranes. I. Fluorescence Depolarization Studies on the Effect of Polymeric Biocide Bearing Biguanide Groups in the Main Chain. *Biochim. Biophys. Acta* **1983**, *735*, 380−386.
(14) Ikeda, T.; Ledwith, A.; Bamford, C. H.; Hann, R. A. Interaction of a Polymeric Biguanide Biocide with Phospholipid Membranes. *Biochim. Biophys. Acta* **1984**, *769*, 57−66.
(15) Timofeeva, L.; Kleshcheva, N. Antimicrobial Polymers: Mechanism of Action, Factors of Activity, and Applications. *Appl. Microbiol. Biotechnol.* **2011**, *89*, 475−492.
(16) Goodman, C. M.; McCusker, C. D.; Yilmaz, T.; Rotello, V. M. Toxicity of Gold Nanoparticles Functionalized with Cationic and Anionic Side Chains. *Bioconjugate Chem.* **2004**, *15*, 897−900.
(17) Lienkamp, K.; Madkour, A. E.; Musante, A.; Nelson, C. F.; Nusslein, K.; Tew, G. N. Antimicrobial Polymers Prepared by ROMP with Unprecedented Selectivity: A Molecular Construction Kit Approach. *J. Am. Chem. Soc.* **2008**, *130*, 9836−9843.
(18) Lienkamp, K.; Tew, G. N. Synthetic Mimics of Antimicrobial Peptides-a Versatile Ring-Opening Metathesis Polymerization Based Platform for the Synthesis of Selective Antibacterial and Cell-Penetrating Polymers. *Chem. - Eur. J.* **2009**, *15*, 11784−11800.
(19) Al-Ahmad, A.; Laird, D.; Zou, P.; Tomakidi, P.; Steinberg, T.; Lienkamp, K. Nature-Inspired Antimicrobial Polymers − Assessment of Their Potential for Biomedical Applications. *PLoS One* **2013**, *8*, No. e73812.
(20) Zou, P.; Laird, D.; Riga, E. K.; Deng, Z.; Dorner, F.; Perez-Hernandez, H.-R.; Guevara-Solarte, D. L.; Steinberg, T.; Al-Ahmad, A.; Lienkamp, K. Antimicrobial and Cell-Compatible Surface-Attached Polymer Networks − How the Correlation of Chemical Structure to Physical and Biological Data Leads to a Modified Mechanism of Action. *J. Mater. Chem. B* **2015**, *3*, 6224−6238.
(21) Dorner, F.; Boschert, D.; Schneider, A.; Hartleb, W.; Al-Ahmad, A.; Lienkamp, K. Toward Self-Regenerating Antimicrobial Polymer Surfaces. *ACS Macro Lett.* **2015**, *4*, 1337−1340.
(22) Kurowska, M.; Eickenscheidt, A.; Guevara-Solarte, D. L.; Widyaya, V. T.; Marx, F.; Al-Ahmad, A.; Lienkamp, K. A Simultaneously Antimicrobial, Protein-Repellent, and Cell-Compatible Polyzwitterion Network. *Biomacromolecules* **2017**, *18*, 1373−1386.
(23) Hartleb, W.; Saar, J. S.; Zou, P.; Lienkamp, K. Just Antimicrobial Is Not Enough: Toward Bifunctional Polymer Surfaces with Dual Antimicrobial and Protein-Repellent Functionality. *Macromol. Chem. Phys.* **2016**, *217*, 225−231.
(24) Lienkamp, K.; Kumar, K.; Som, A.; Nusslein, K.; et al. "Doubly Selective" Antimicrobial Polymers: How Do They Differentiate. *Chem. - Eur. J.* **2009**, 11710−11714.
(25) Lienkamp, K.; Madkour, A. E.; Kumar, K.-N.; Nusslein, K.; Tew, G. N. Antimicrobial Polymers Prepared by Ring-Opening Metathesis Polymerization: Manipulating Antimicrobial Properties by Organic Counterion and Charge Density Variation. *Chem. - Eur. J.* **2009**, *15*, 11715−11722.
(26) Trnka, T. M.; Grubbs, R. H. The Development of L2X2Ru = CHR Olefin Metathesis Catalysts: An Organometallic Success Story. *Acc. Chem. Res.* **2001**, *34*, 18−29.
(27) Jana, N. R.; Gearheart, L.; Murphy, C. J. Seeding Growth for Size Control of 5−40 Nm Diameter Gold Nanoparticles. *Langmuir* **2001**, 6782−6786.
(28) Liposome Preparation|Avanti Polar Lipids. https://avantilipids.com/tech-support/liposome-preparation/ (accessed Jan 5, 2017).
(29) Haiss, W.; Thanh, N. T. K.; Aveyard, J.; Fernig, D. G. Determination of Size and Concentration of Gold Nanoparticles from UV-Vis Spectra. *Anal. Chem.* **2007**, *79*, 4215−4221.
(30) Mansfield, E.; Tyner, K. M.; Poling, C. M.; Blacklock, J. L. Determination of Nanoparticle Surface Coatings and Nanoparticle Purity Using Microscale Thermogravimetric Analysis. *Anal. Chem.* **2014**, 1478−1484.
(31) Bartczak, D.; Kanaras, A. G. Preparation of Peptide-Functionalized Gold Nanoparticles Using One Pot EDC/Sulfo-NHS Coupling. *Langmuir* **2011**, 10119−10123.
(32) Kelly, K. L.; Coronado, E.; Zhao, L.; Schatz, G. C. The Optical Properties of Metal Nanoparticles: The Influence of Size, Shape, and Dielectric Environment. *J. Phys. Chem. B* **2003**, *107*, 668−677.
(33) Burchard, W. Static and Dynamic Light Scattering Approaches to Structure Determination of Biopolymers. *Laser Light Scattering in Biochemistry*; Royal Society of Chemistry, 1992; pp 3−22.
(34) Spampinato, V.; Parracino, M. A.; La Spina, R.; Rossi, F.; Ceccone, G. Surface Analysis of Gold Nanoparticles Functionalized with Thiol-Modified Glucose SAMs for Biosensor Applications. *Front. Chem.* **2016**, *4*, 8.
(35) Torelli, M. D.; Putans, R. A.; Tan, Y.; Lohse, S. E.; Murphy, C. J.; Hamers, R. J. Quantitative Determination of Ligand Densities on Nanomaterials by X-Ray Photoelectron Spectroscopy. *ACS Appl. Mater. Interfaces* **2015**, *7*, 1720−1725.
(36) Hong, J.; Hamers, R. J.; Pedersen, J. A.; Cui, Q. A Hybrid Molecular Dynamics/Multiconformer Continuum Electrostatics (MD/MCCE) Approach for the Determination of Surface Charge of Nanomaterials. *J. Phys. Chem. C* **2017**, 3584−3596.
(37) Cameron, G. G. Polyelectrolytes: Formation, Characterization and Application. H. Dautzenberg, W. Jaeger, J. Kotz, B. Philipp, Ch. Seidel and D. Stscherbina. Carl Hanser Verlag: Munich, 1994. Pp. Xiv + 343, Price DM168.00. ISBN 1-56990-127-9. ISBN 3-446-17127-4. *Polym. Int.* **1995**, *38*, 106.

DOI: 10.1021/acs.langmuir.7b04285
Langmuir 2018, 34, 4614−4625